Journal Pre-proofs

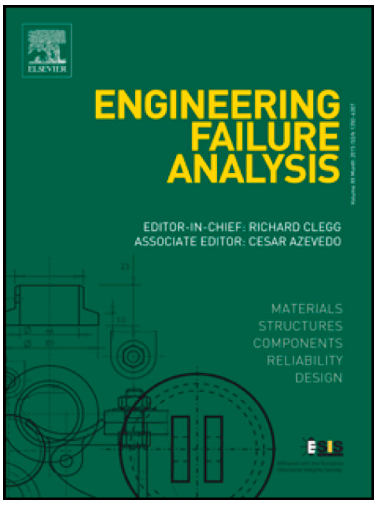

Corrosion behavior of HVOF sprayed WC-10Co4Cr coatings in the simulated seawater drilling fluid under the high pressure

Yong-kuan Zhou, Xiao-bin Liu, Jia-jie Kang, Wen Yue, Wen-bo Qin, Guo-zheng Ma, Zhi-qiang Fu, Li-na Zhu, Ding-shun She, Hai-dou Wang, Jian Liang, Wei Weng, Cheng-biao Wang

PII: S1350-6307(19)31005-2
DOI: https://doi.org/10.1016/j.engfailanal.2019.104338
Reference: EFA 104338

To appear in: *Engineering Failure Analysis*

Received Date: 14 July 2019
Revised Date: 3 October 2019
Accepted Date: 19 November 2019

Please cite this article as: Zhou, Y-k., Liu, X-b., Kang, J-j., Yue, W., Qin, W-b., Ma, G-z., Fu, Z-q., Zhu, L-n., She, D-s., Wang, H-d., Liang, J., Weng, W., Wang, C-b., Corrosion behavior of HVOF sprayed WC-10Co4Cr coatings in the simulated seawater drilling fluid under the high pressure, *Engineering Failure Analysis* (2019), doi: https://doi.org/10.1016/j.engfailanal.2019.104338

Corrosion behavior of HVOF sprayed WC-10Co4Cr coatings in the simulated seawater drilling fluid under the high pressure

Yong-kuan Zhou [a], Xiao-bin Liu [a], Jia-jie Kang [a,b,f]*, Wen Yue [a,f], Wen-bo Qin [a], Guo-zheng Ma[c]**, Zhi-qiang Fu [a,f], Li-na Zhu [a,f], Ding-shun She [a,f], Hai-dou Wang [a,c], Jian Liang [a,d], Wei Weng [e], Cheng-biao Wang [f,g]

[a] *School of Engineering and Technology, China University of Geosciences (Beijing), Beijing 100083, China*

[b] *Key Laboratory of Deep GeoDrilling Technology of Ministry of Natural Resources, Beijing 100083, China*

[c] *National Key Lab for Remanufacturing, Academy of Armored Forces Engineering, Beijing 100072, China*

[d] *Institute of Exploration Techniques, Chinese Academy of Geological Sciences, Langfang 065000, China*

[e] *Beijing Institute of Exploration Engineering, China Geological Survey, Beijing 100083, China*

[f] *Zhengzhou Institute, China University of Geosciences (Beijing), Zhengzhou 451283, China*

[g] *Zhengzhou Institute of Multipurpose Utilization of Mineral Resources, Chinese Academy of Geological Sciences, Zhengzhou 450006, China*

* Corresponding author. Tel.: +86 10 82321981; fax: +86 10 82322624.

E-mail address: kangjiajie@cugb.edu.cn (J.J. Kang); magz0929@163.com (G.Z. Ma)

Abstract: Two kinds of WC-10Co4Cr composite coatings with conventional (micron-sized WC particles) and bimodal (a mixture of nano-sized and micron-sized WC particles) structures were successfully prepared on 35CrMo steel (ANSI/ASTM 4135) substrate by high velocity oxygen fuel (HVOF) technology. Scanning electron microscope (SEM) equipped with the energy dispersive spectroscopy (EDS), mechanical testing machine, microhardness tester were used to analyze the

characteristics of the coatings. The coatings were immersed in the simulated seawater drilling fluid under the high pressure to simulate the deep-sea environment, and then electrochemical impedance spectroscopy (EIS), potentiodynamic polarization were carried out to investigate the electrochemical properties of the coatings and substrate. The results show the WC-10Co4Cr coating has excellent corrosion resistance and can effectively protect the substrate under the high pressure. Besides, compared with the conventional coating (CC), the bimodal coating (BC) has a denser microstructure, more excellent mechanical properties, lower porosity, and better corrosion resistance. The corrosion mechanism of the coatings in the simulated seawater drilling fluid under high the pressure is as follows: The micro-galvanic corrosion between the WC phase and the CoCr binder phase is the primary corrosion mechanism. Besides, the electrolyte under the high pressure is more penetrable, so the crevice corrosion also exists.

Key words: High velocity oxygen fuel; WC-10Co4Cr; Conventional; Bimodal; Corrosion resistance

1. Introduction

With the depletion of land resources, the energy exploration of marine resources is increasing. Therefore, drilling equipment is indispensable, such as drill bits, drill pipes, drill pipe joints and stabilizers. High-pressure corrosive environment for deep sea exploration puts forward higher requirements on the corrosion resistance of drilling equipment [1-3]. However, the corrosion mechanism of materials in the deep sea environment is quite different from that under atmospheric pressure, so the corrosion performance of materials under deep sea conditions should be considered [4].

The metal ceramic coating is an excellent wear-resistant coating with comprehensive properties. It can enhance hardness and strength from the hard carbide phase, while it provides toughness and plasticity by the metal binder phase. Therefore, it possesses the

combined characteristics of ceramic and metal materials. Traditional metal ceramic coatings include WC-Co, WC-CoCr, CrC-NiCr, and Al_2O_3-TiO_2/ NiMoAl. Among them, WC is the most widely used materials. High Velocity Oxygen Fuel (HVOF) has the advantages of high velocity, low flame temperature, good coating quality and high bond strength with substrate. WC based ceramic coating has good mechanical properties, wear and corrosion resistance, high hardness and low porosity. Besides, HVOF sprayed WC metal ceramic coating ensures more powder feed, low oxidation and decarburization in the spraying process. Consequently, the high bond strength, hardness, compactness and wear resistance were achieved [5-10]. However, deep-sea drilling requires not only the wear resistance of the drill but also the corrosion performance.

Perry et al [11] found that the addition of chromium to a cobalt matrix increases the corrosion resistance of a WC-based HVOF sprayed cermet coating. HVOF-sprayed coatings (particularly WC–10Co4Cr cermet coating) possess a superior corrosion resistance than ordinary chrome platings in the aggressive 0.1 N HCl solution [12]. The comparison of the corrosion resistance of WC-10Co4Cr coatings and hard chromium coatings in 3.5 wt. % NaCl solution demonstrated that the WC-10Co4Cr coatings have better corrosion resistance [13]. Cr would be oxidized to Cr_2O_3 in the coating, which can retard the corrosion process in 3.5 wt. % NaCl solution [14]. Stack et al [15] found that the WC based cermet coating passivates in acidic environment, and the corrosion resistance decreases with the increase of pH value. WC would be oxidized to WO_3 in acidic environment to interfere corrosion, but would react with OH^- in alkaline environment to generate WO_4^{2-}, so the corrosion rate of coatings in alkaline environment is higher than that of in acidic environment [16]. The research of Picas et al [17] indicated the bonding phase of WC-CoCr coatings would dissolve in the solution

of 1mol/L acidic solution. In addition, gap corrosion may occur when the interface of the coating is immersed in the acidic solution.

Recent research shows that the corrosion performance of HVOF-sprayed cermet coatings can be improved by reducing the carbide particle size to nano scale [18-20]. These improvements have been attributed to various reasons, such as more uniform composition of the binder, denser distribution of the carbide phase and higher dissolution of W and C into the binder [21]. However, with the decreases of carbide size, nanostructured WC-Co powder decarburized in the spraying process, which should be avoided as much as possible. Bimodal powders have been produced to minimize this effect, keeping higher resistance to corrosion when compared with conventional ones [22-24].

Previous work has reported the corrosion behavior of conventional and nanostructured coatings [25-27], but there is few research on bimodal coatings, especially the corrosion behavior under the high pressure conditions. In the present study, the conventional coatings (CC) and bimodal coatings (BC) are prepared by two different powder particles deposited with HVOF technology on 35CrMo steel (ANSI/ASTM 4135) substrate. The aim of this work is to evaluate the corrosion behavior of the WC-10Co4Cr coatings in the simulated seawater drilling fluid, which can simulate marine drilling environments. The results of this work will provide scientific guidance for the surface hardening and failure analysis of drilling tools served in deep sea drilling.

2. Experimental methods

2.1 Coating preparation

In this study, two commercially available powders were selected as feedstock, which were produced by BGRIMM Technology Group. The powders were conventional WC-

10Co4Cr and bimodal WC-10Co4Cr, which were prepared by agglomeration and sintering. The proportion of the powder component is: WC-86 wt. %, Co-10 wt. % and Cr-4 wt. %, and the size of two powders is basically the same. The difference is the bimodal powders consist on a mixture of nano-sized (~30%) and micron-sized WC particles while the size of the WC particles in conventional powders are micron. The size range of micron-sized WC particles is 0.2-1.3 μm, and the size range of nano-sized WC particles is 70–200 nm in bimodal powders respectively. Besides, the size range of micron-sized WC particles is 0.7-1.3 μm in conventional powders. The composition of the powders is shown in Table 1. The 35CrMo steel (chemical composition: C: 0.18-0.40, Si: 0.17-0.37, Mn: 0.40-0.70, Cr: 0.80-1.10, and balance Fe) was used as the coated substratewith the size of 40 mm×20 mm×5 mm. In order to conveniently process, the substrate has been chamfered, and the chamfer angle is 45°, the chamfer length is 1 mm. Before spraying, the substrate surfaces were degreased and sandblasted, and the substrate was cleaned in an ultrasonic cleaning apparatus for 30 minutes. The blasting material is corundum with size of 0.3mm. The distance and angle of sand blasting are 300 mm and 70 degrees, respectively. Besides, the substrate needed to be preheated for better bond strength, and the preheating temperature was 150°C, the preheating speed was 0.8 m/s. The spraying was carried out using the GTV MF-P-HVOF-FP-K 2000 HVOF system (GTV Impex GmbH, Germany) equipped with a GTV HVOF K2 spray gun. The thickness of the WC-10Co4Cr coatings are in a range of 200~300 μm. The CC and BC refer to the conventional coating and the bimodal coating, respectively. The HVOF process parameters are shown in Table 2.

Table 1. Composition of two WC-10Co4Cr powders.

Powder type	Manufacturing method	Nano WC size D/nm	Micro WC size D/μm	Powder size D/μm	Nano WC rate/ %
Bimodal	Agglomeration	70–200	0.2-1.3	15-45	30
Conventional	Agglomeration		0.7-1.3	15-45	0

Table 2. HVOF process parameters.

Process parameters	Oxygen flow rate	Spray distance	Powder feed rate	Kerosene flow rate	Nitrogen flow rate	Spray speed	Pitch distance
Values	90 L/min	420 mm	100 g/min	26 L/min	9 L/min	0.5 m/s	5 mm

2.2 Coating characterization

The morphologies of the powders and the WC-10Co4Cr coatings before and after the immersion were observed by SEM (MERLIN Compact, ZEISS, Germany), and the composition of the coatings was analyzed by energy dispersive spectroscopy (EDS). By the method of the reference intensity ration (RIR) method, the MDI jade 6.0 software was used to semi-quantitatively calculate the amount of each phase in the powders and coatings. According to the national standard GB8642-2002, the bond strength of the coating was tested. The coated samples were bonded to 35CrMo steel using E7 glue. After solidification, the coating was applied to a universal tensile test apparatus. The sample was stretched at the rate of 1 mm/min. The test results were taken from the average of 5 sets of parallel samples. The combined strength was calculated as follows [28]:

$$R_H = F_M/S \quad (1)$$

Where R_H is the bond strength (MPa); F_M is the maximum load (N); S is the cross-sectional area of the fracture surface (mm^2)

The porosity of the coating was measured using a gray scale method, and the values were evaluated using the *ImageJ2x* software. The phase composition of the powders and the coatings was characterized by X-ray diffraction (XRD, AXS D-8, Bruker, Germany) apparatus with CuKα radiation and the scanning rate was 4°/min with the 2θ range from 20° to 90°. The microhardness of the coating was measured using a microhardness tester (MICROMET-6030, Buehler, America) with a load of 2.94 N and a hold time of 15 seconds. In order to ensure the stability of the data, the microhardness value is the average of 5 measurement points. The surface roughness (Ra) value of the coating was measured by a 3D measuring laser microscope (OLS4000, OLYMPUS, Japan).

2.3 Electrochemical corrosion tests

The immersion conditions are as follows: continuous immersion in the simulated seawater drilling fluid for different time, such as 1 day, 7 days, 15 days at room temperature (about 15°C). The simulated seawater drilling fluid composition is shown in Table 3, and a certain amount of NaOH were added to configure the simulated seawater drilling fluid with the pH of 9. The experimental device is shown in Fig.1.

Table 3. Composition of the simulated seawater drilling fluid.

Composition	NaCl	Anti-bentonite	Filtrate reducer	Na_2CO_3
Content	3.5%	2%	1%	0.25%

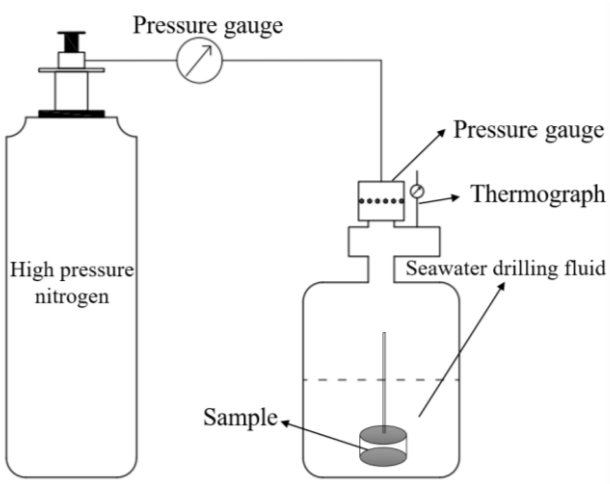

Fig. 1. Schematic diagram of immerse test apparatus.

The electrochemical behavior of the coating samples was examined at room temperature (about 15°C) in the simulated seawater drilling fluid, using the ZAHNER IM6ex electrochemical measurement system in a three-electrode test cell. The sample was taken as the working electrode, a platinum wire as a counter electrode and a saturated calomel electrode as a reference electrode. The specimens for electrochemical tests were closely encapsulated in a non-conducting epoxy resin with the back side of the specimen connected by a wire, leaving only an area of 1.0 cm^2 exposed to the electrolyte. The electrochemical tests include the measurement of the open circuit potential (OCP), potentiodynamic polarization tests and electrochemical impedance spectroscopy (EIS). These tests were conducted to compare the corrosion resistance of 35CrMo, CC and BC. The samples were immersed in the simulated seawater drilling fluid for 30 mi before testing to completely wet the surface of the coating and stabilize the OCP. As the OCP became steady, potentiodynamic polarization curves were measured with a fixed sweep rate of 1 mV/s in the scanning voltage range of -300mV-0V. The corrosion current density (i_{corr}) and corrosion potential (E_{corr}) were obtained by linear fitting with the intersection of the anode and cathode polarization curves, according to the Tafel extrapolation technique. EIS test was conducted at the OCP by

applying a sinusoidal potential excitation of 5 mV amplitude in the frequency range from 100 kHz to 10 MHz [17, 29, 30]. Each test was repeated at least three times to make sure a good repeatability of the experiment results.

3 Results and discussion

3.1 Characterisation of coatings

Fig. 2 shows the surface morphology of conventional and bimodal powders. The conventional and bimodal powders were both made by agglomerating and sintering, as is shown Fig. 2(a) and (c), two powders are similar in appearance, exhibiting a spherical or ellipsoidal shape, and the surface of the powder particles is loose and porous. As can be seen from the enlarged figure, the bimodal powder is less hollow and the powder size is more similar than the conventional powder. From Fig. 2(b) and Fig. 2(d) we can see the shape of the WC particles is irregular and blocky in the conventional powders and the bimodal powders [10]. The coatings prepared from these powders are tightly bonded because the powders have good flowability during the spraying process.

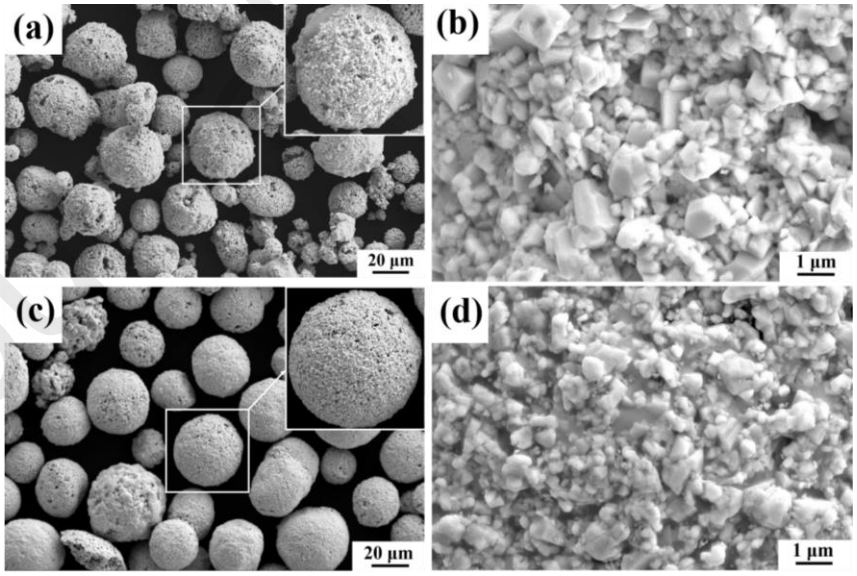

Fig. 2. SEM images of WC-10Co4Cr powders.

(a) Conventional powders ; (b) The magnification of conventional powders;

(c) Bimodal powders; (d) The magnification of bimodal powders

Fig. 3(a) and Fig. 3(d) show the cross-sectional morphologies of the CC and BC. The coatings are tightly bonded to the substrate. The interfaces are typical mechanical bonding with no obvious defects. The interior of the coating exhibits a relatively tight layered structure. The light contrast areas are WC hard phases, and the dark contrast areas between the particles are mainly CoCr binder phases [2, 10]. As exhibited in Fig. 3(b) and Fig. 3(e), WC particles maintain the original polygonal shape during spraying process. There are also a few internal pores among WC particles due to the impact of the small WC particles on the substrate at high speeds during HVOF spraying. In the BC, the nano-sized WC particles are dispersed in the gaps of micro-sized WC particles gap or partially aggregated near the binder phase. Fig. 3(c) and Fig. 3(f) show the morphologies of sprayed samples have unmelted particles. The BC has less unmelted particles than CC. Due to the relatively low flame temperature and high flight speed during HVOF spraying, it results that the large WC particles was incompletely melted. Therefore, The CC with micron WC particles are only softened on the surface. The BC contains nano-sized powder particles which due to their small particle size, are softened by heat during spraying and are severely deformed when colliding with the substrate to fully spread on the surface of the substrate.

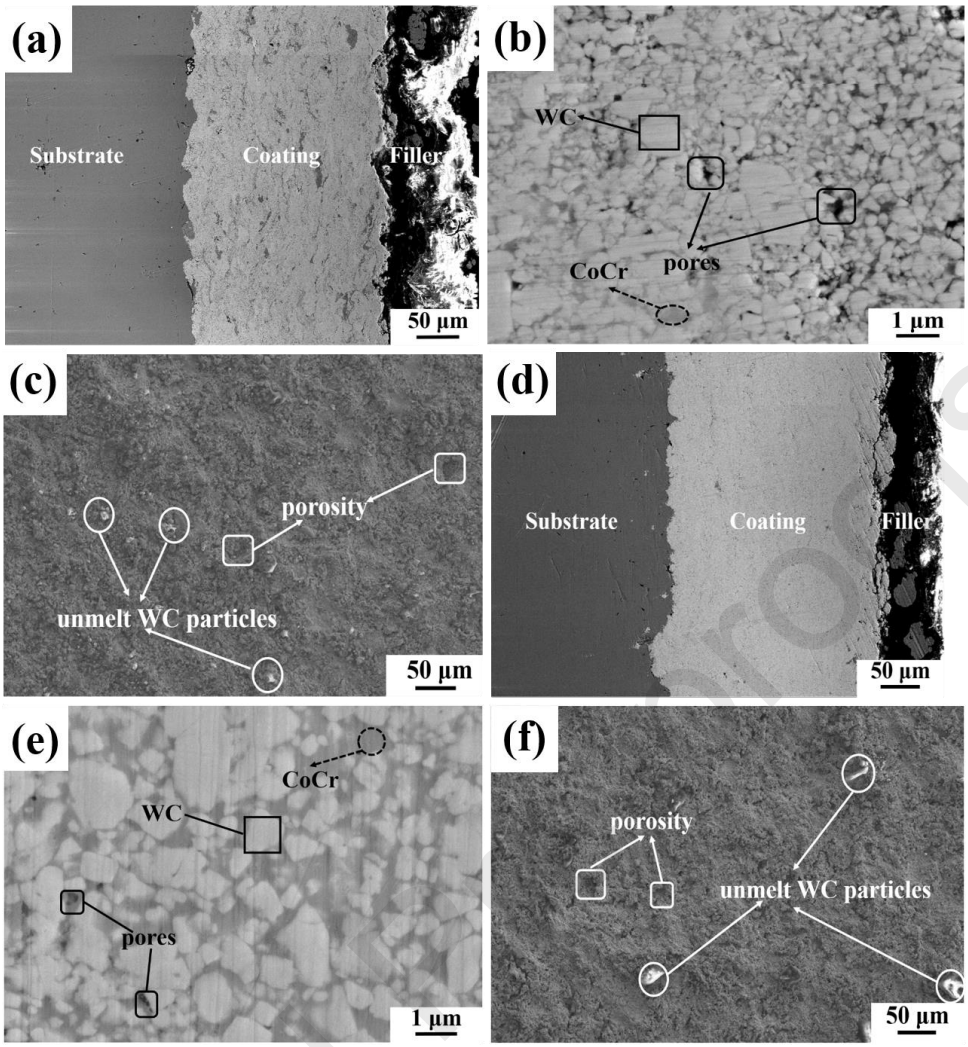

Fig. 3. SEM images of WC-10Co4Cr coating.

(a) The cross-section of the CC; (b) The magnification of cross-section of the CC;

(c) The surface of the CC; (d) The cross-section of the BC;

(e) The magnification of cross-section of the BC; (f) The surface of the BC

As shown in Fig. 4, for the conventional structure and the bimodal structure of WC-10Co4Cr, their phase compositions are basically in common. The strongest peak in XRD spectrum is the diffraction peak of WC phase, indicating that the main phase is WC. However, the coating displays a new W_2C diffraction peak at about 38° of 2θ, and the formation of W_2C is produced by the dissolution of WC into the binder phase during spraying process and subsequently oxidation and precipitation reactions, indicating that some oxidation and decarburization occurred in the WC phase during the spraying

process [31, 32]. The content of W2C in the BC and CC was measured to be 3.18 % and 4.86 % by RIR method respectively, it can be found the mass fraction of W2C in the BC is slightly higher than that of the CC. This is because the nano-sized WC has larger specific surface area than micro-grade WC, so it is easier to oxidation and decarburization. The presence of W2C leads to increased brittleness of the coating and affects corrosion resistance [33, 34].Co is partially converted to amorphous phase and/or evaporated during HVOF spraying. As can be seen in larger graphs of Fig. 4, the XRD patterns for CC and BC show broad peaks at 2θ= 37–47°, indicating that amorphous or nanocrystalline phases has formed [35]. The amorphous or nanocrystalline binder phase resulted from (a) the rapid cooling of the splats that inhibits microcrystal development and/or (b) the supersaturation of the binder by W and C diffused into/ dissolved in the binder phase [20, 22, 36].The diffraction peak of Co3W3C is found in the XRD pattern of the coating, which was due to the bonding of the WC particles and the CoCr binder phase during solid state sintering [10].

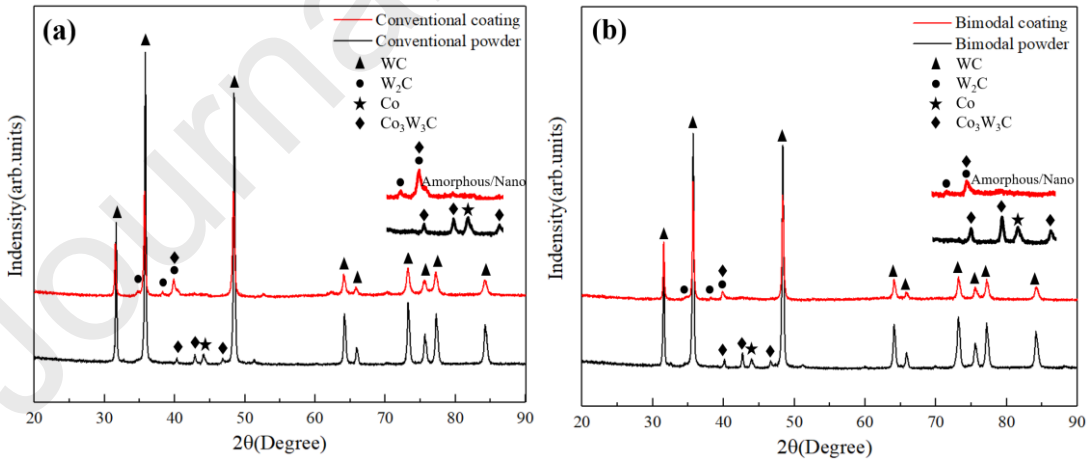

Fig. 4. XRD patterns of the HVOF WC-10Co4Cr powers and coatings.

(a) Conventional; (b) Bimodal

The porosity, roughness values and microhardness were measured as shown in Table

4. The porosity and roughness value of the BC is lower than that of the CC, indicating the bimodal molten particles are sufficiently flat on the substrate to form a more compact coating structure. The lower value of porosity and roughness of the BC is attributed to the fact that the average size of the WC particle is less than that of the CC. The nano-sized WC particles in the BC melt well during HVOF spraying and are severely deformed after impacting the substrate or pre-coating, and the flattening is superior to the micron WC particles. Table 4 also shows the microhardness of the 35CrMo steel substrate and WC-10Co4Cr coatings. It can be seen from the table the average microhardness of the BC and CC is 1292 $HV_{0.3}$ and 1244 $HV_{0.3}$, respectively. The microhardness of coatings is about four times than that of the substrate (278 HV0.3). This is mainly due to the uniform distribution of the WC hard phase. The greater the specific surface area of the hard phases in the coating and the more uniform of the distribution, the higher the microhardness of the coating, so the BC have a higher microhardness than that of the CC. The WC phase in the BC coatings occupies a higher specific surface area due to the finer particle size. Moreover, the nano-sized WC particles are evenly distributed around the WC, which acts as a dispersion strengthening and fine grain strengthening. In addition, the bond strength test of the WC-10Co4Cr coatings shows that the average bond strength is approximately 68 MPa, indicating the WC-10Co4Cr coatings prepared by HVOF have a good bond strength [24].

Table 4. The porosity, roughness values and microhardness of the CC and BC.

	Porosity (%)	As-sprayed roughness (R_a μm）	Average microhardness ($HV_{0.3}$)
35CrMo			278±25
CC	1.6 ± 0.1	5.1 ± 0.5	1244± 45
BC	1.3 ± 0.1	3.2 ± 0.6	1292 ± 50

3.2 Electrochemical Corrosion Behavior

3.2.1 Potentiodynamic Polarization Curves

Fig. 5 shows the polarization curves of the CC, the BC and 35CrMo. The corresponding electrochemical parameters are shown in Table 5. According to Fig. 5 and Table 5, the corrosion potentials (E_{corr}) of 35CrMo was -0.639 V with a corrosion current density (i_{corr}) about 17.82×10^{-2} μA•cm^{-2}. For CC, of the E_{corr} and i_{corr} was -0.525 V and 3.06 μA•cm^{-2}, respectively. As for BC, E_{corr} shifted to positive potential (-0.478 V) with a decrease of i_{corr} (2.42 μA•cm^{-2}). Generally, a lower i_{corr} and a higher E_{corr} indicated better corrosion resistance. Due to the passivation film formation effect of Cr and the noble phase of WC, the corrosion potential of WC-CoCr coating is higher than that of the substrate [37, 38]. It can be found the coatings can effectively protect the substrate. The BC had better corrosion resistance because the BC has lower porosity and more uniform microstructure can hinder the permeation of electrolyte and enhance the corrosion property of coatings [20].

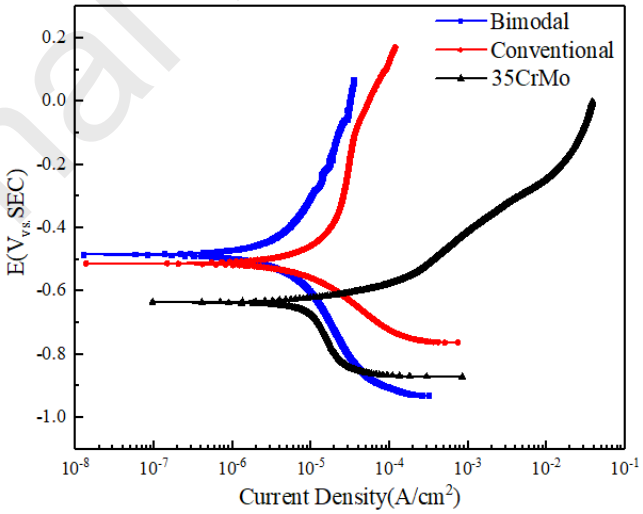

Fig. 5. Potentiodynamic polarisation curves of the 35CrMo substrate and two WC-10Co4Cr coatings in the simulated seawater drilling fluid in the simulated seawater drilling fluid under atmospheric pressure.

Table 5. Electrochemical values extracted from the polarization curves. Ecorr: corrosion potential; icorr: corrosion current density from Tafel extrapolation; bc: cathodic Tafel slope value; ba: and anodic Tafel slope value

Materials	Ecorr (V)	icorr ($\mu A \cdot cm^{-2}$)	bc (mV/decade)	ba (mV/decade)
35CrMo	-0.639 ± 0.007	17.82 ± 0.44	1620 ± 50	95 ± 4
CC	-0.525 ± 0.005	3.06 ± 0.07	144 ± 5	237 ± 8
BC	-0.478 ± 0.004	2.42 ± 0.05	210 ± 5	278 ± 8

3.2.2 EIS Plots of the Coatings

EIS measurements were conducted to detecte the corrosion behavior of coatings. Fig. 6 show the EIS plots of the CC and BC. In the Nyquist plot, the electrochemical impedance spectroscopy shows a similarly deformed semicircle, indicating that their failure modes in the simulated seawater drilling fluid are consistent, and the sequence of the radius of the deformed semicircle is: BC > CC> 35CrMo. A large diameter of deformed semicircle suggests an excellent barrier property [39, 40]. As can be seen from the Bode-impedance plot, the sequence of the impedance values is: BC (10042 Ω) > CC (3302 Ω) > 35CrMo (1314 Ω). In the Bode-impedance plot, the lowest frequency (|Z|0.01Hz) impedance modulus is used as a semi-quantitative indicator of the corrosion resistance of the coating [41]. It is indicated that the sequence of the electron transfer rate in the simulated seawater drilling fluid is: BC < CC < 35CrMo. The comparisons of corrosion rates are as follows: BC < CC < 35CrMo, so the BC has the best corrosion resistance, which is also consistent with the results of the dynamic polarization curve.

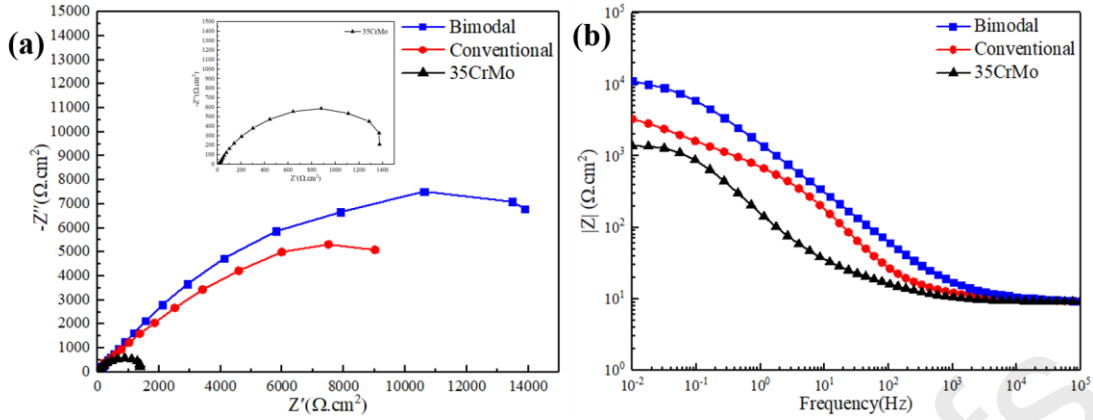

Fig. 6. EIS of the CC and BC by (a) Nyquist plot; (b) Bode-impedance plot in the simulated seawater drilling fluid under atmospheric pressure.

The Fig. 7 (a) and (c) are the Nyquist plot and Bode-impedance plot of the BC immersed in the simulated seawater drilling fluid for 1 day, 7 days and 15 days under the high pressure of 5 MPa. The sequence of the diameter of the capacitive anti-arc is: 1 day> 7 days > 15 days. Besides, it can be seen that the sequence of the resistance at the same frequency is: 1 day > 7 days > 15 days. So the sequence of the transfer rate of electrons of BC is: 15 days > 7 days > 1 day. For the BC, the radii of capacitive arcs decrease monotonously with immersion time, indicating that the coating has reduced corrosion resistance with the immersion time under the high pressure of 5 MPa. As can be seen from Fig. 7 (b) and (d), the CC also shows similar trends. However, it is found that the same anti-corrosion diameter of the BC is larger than that of the CC in the same condition. Also, in the case of immersion for the same time the resistance of the BC is greater than that of the CC, that is, the electron transfer rate of the BC is smaller than that of the CC, and the corrosion of the BC is slightly lower than the corrosion of the CC. The corrosion resistance of the coatings decreases with the immersion time because the corrosion solution is more permeable in the high pressure environment. Besides, BC has a lower porosity and more uniform structure, it can effectively hinder the

penetration of the drilling fluid and improve the corrosion resistance of the coating, so the BC has better corrosion resistance than the CC.

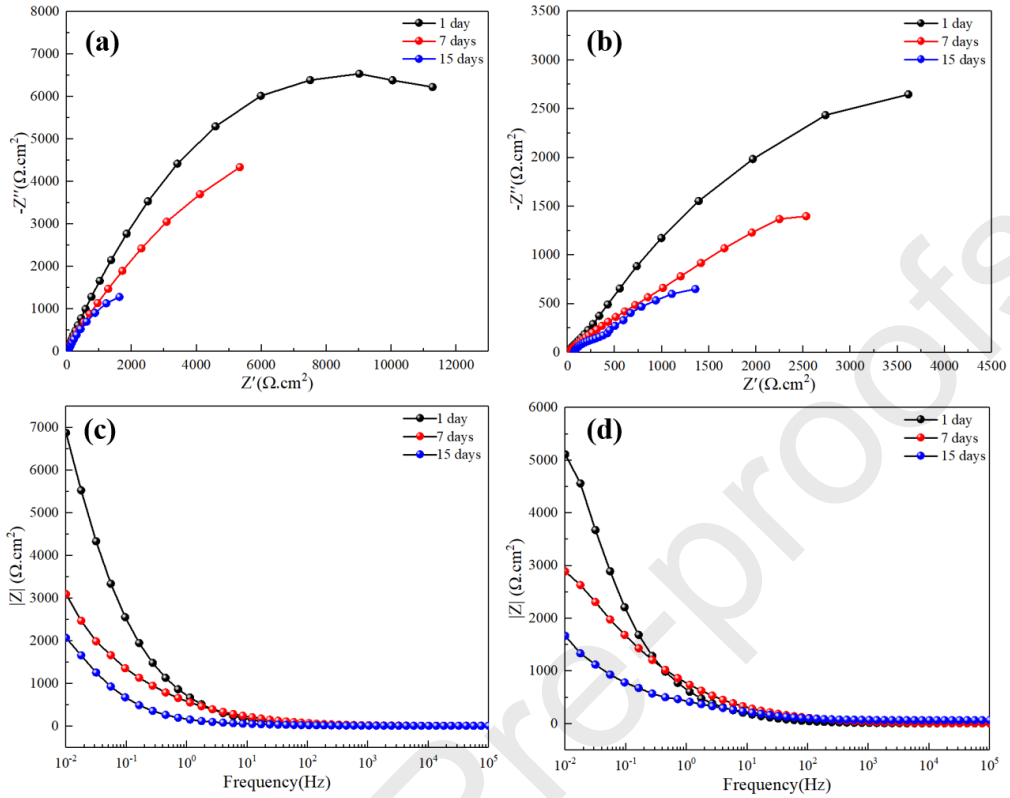

Fig. 7. EIS of the WC-10Co4Cr coatings on 1 day, 7 days and 15 days in the simulated seawater drilling fluid under the high pressure of 5 MPa. (a) Nyquist Plot of the BC; (b) Nyquist Plot of the CC; (c) Bode-impedance plot of the BC; (d) Bode-impedance plot of the CC

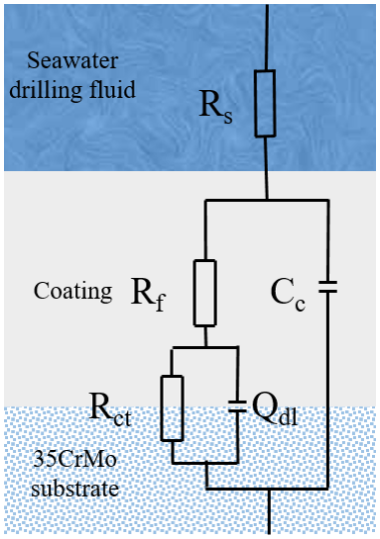

Fig. 8. Equivalent circuit model of the corrosion of the conventional and bimodal WC-10Co4Cr coatings.

The EIS results are further fitted by *ZsimpWin* software to understand the corrosion performance of the coatings, and the corresponding equivalent electric circuit model is shown in Fig. 8. In this model, R_s, R_f, and R_{ct} represents the solution resistance, coating pore resistance, and charge transfer resistance, respectively. C_c and Q_{dl} represents coating capacitance and double-layer capacitance, respectively. Similar equivalent circuit has been reported by other researchers [13, 42]. Table 6 shows the fitted results for EIS of the HVOF-sprayed CC and BC. With the prolongation of the immersion time in the simulated seawater drilling fluid, the pore resistance of the BC and the CC gradually decreased. Coating pore resistance (R_f) can reflect the change of corrosion performance clearly [43, 44]. After the immersion for 1 day, 7 days and 15 days, the pore resistance of the BC decreased from 7895 Ω (when not immersed) to 5036 Ω, 4289 Ω and 3509 Ω, respectively. After the immersion for 1 day, 7 days and 15 days, the pore resistance of the CC decreased from 6586 Ω (when not immersed) to 4248 Ω, 3399 Ω and 2766 Ω, respectively. Consequently, the BC has a better corrosion resistance. It is indicated that the pores on the surface of the coating hindered the decrease of electron mobility. That is, the porosity of the coating surface increased because the CoCr binder phase dissolved into the drilling fluid in an alkaline environment. When the binder phase around WC was dissolved in a large amount, it may cause the WC phase to fall off, further increasing the surface porosity of the coating [45, 46].

Table 6. Electrochemical fitting of the conventional and bimodal WC–10Co4Cr coatings.

	R_s(Ω cm^2)	C_c (F cm^{-2} s^{-n})	N1	R_f(Ω cm^2)	Q_{dl}(F cm^{-2} s^{-n})	N2	R_{ct}(Ω cm^2)
CC (30 mins)	10.63	9.632E-5	0.8342	6586	8.928E-4	0.8	3.594E4
CC (1 day)	8.061	6.555E-4	0.6884	4248	5.557E-4	0.6082	2.117E4
CC (7 days)	6.234	3.611E-4	0.5845	3399	0.0001097	0.6113	1.402E4
CC (15 days)	7.15	1.943E-4	0.8674	2766	2.235E-3	0.8	8.044E3
BC (30 mins)	9.691	2.532E-4	06924	7895	2.037E-4	0.7224	5.908E4
BC (1 day)	11.22	2.312E-4	0.6402	5036	9.655E-4	0.6683	3.611E4
BC (7 days)	10.27	1.078E-4	0.8274	4289	2.422E-3	0.8245	1.687E4
BC (15 days)	13.46	5.076E-3	0.7823	3509	6.049E-3	0.8425	9.867E3

3.2.3 The corrosion morphologies of the coatings

Fig. 9 shows the corrosion morphologies of the WC-10Co4Cr coating after 15 days of immersion under the high pressure of 5MPa. During the immersion process, the CoCr binder phase is preferentially affected by corrosion due to the lower potential [47, 48]. The CoCr binder phase is the anode, and the WC phase is the cathode. Because the specific surface area of WC phase is significantly higher than that of CoCr phase, the micro-galvanic corrosion is more serious [2, 38, 41].From Fig. 9(a) and Fig. 9(d), as the binder phase corrodes, the WC particles fall out and leave behind small pits at the interface of the two phase. Fig. 9(b) and Fig. 9(e) show that the WC particle edge is obvious at the stress concentration, which indicates that the CoCr binder phase around WC has been dissolved under the action of micro-galvanic corrosion. The dissolution of the binder phase caused the binding force of the WC particles and surrounding CoCr phase to decrease. When the binder phase has been dissolved to a certain extent, WC particles peel off to form spalling. The above reflects the corrosion of the surface morphologies, we also need to know the internal corrosion of the coatings. As can be seen from Fig. 9(e) and Fig. 9(f), the simulated seawater drilling fluid penetrated into the subsurface of the coating along cracks or holes, which can cause corrosion of the subsurface. The subsurface corrosion of the CC is obvious. However, the subsurface of

the BC is slightly corroded. This form of corrosion is the crevice corrosion and has been reported in the previous literature [17, 49]. Besides, the electrolyte under the high pressure is more penetrable, so the crevice corrosion is more serious. The crevice corrosion phenomena cause the formation of small cracks parallel to the surface, which eventually can remove parts of the coatings. It can be seen from the Fig. 9 that the corrosion of the BC is relatively mild compared to the conventional coating, so the BC has better corrosion resistance.

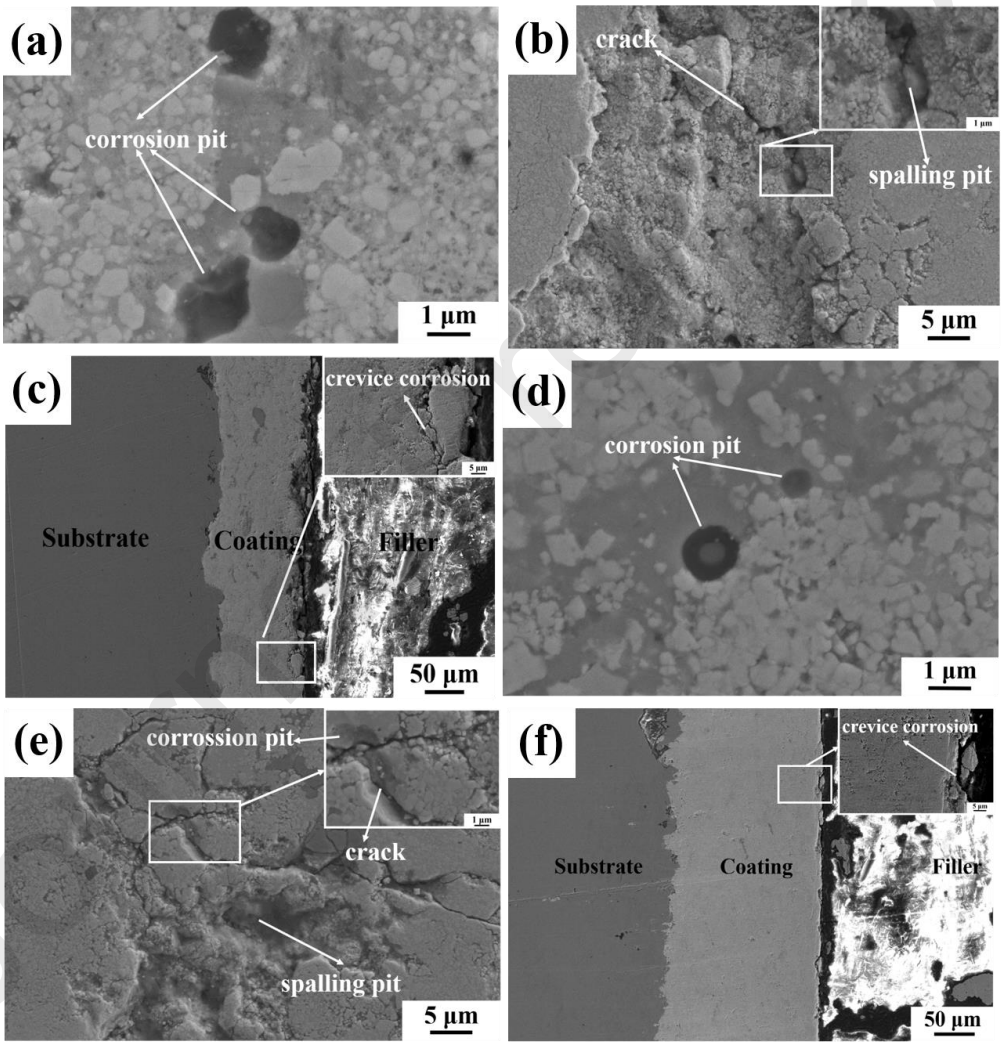

Fig. 9. SEM images of the coatings after 15 days of immersion under the high pressure of 5MPa.

(a) (b) Surface morphologies of the CC (c) Cross section of the CC

(d) (e) Surface morphologies of the BC (f) Cross section of the BC

Previous works by other authors have reported the formation of films on the binder surface based on Co_3O_4, Cr_2O_3 and WO_4^{2-} after corrosion [2, 16, 17, 47]. The EDS analysis of the corrosion pit in Fig. 9(d) is shown in Table 7. The composition is mainly composed of W, C, Co, Cr and O elements, which means that the oxide layers have been formed during the corrosion process. The oxide layers are distributed on the surface in an island shape, which can suppress corrosion performance [38, 50].

The formation of pitting and spalling can further increase the porosity of the coating, resulting in poor corrosion resistance. For the CC and BC, the corrosion resistance of the BC is relatively good due to more uniform microstructure.

Table 7. The element contents of the corrosion pits of Fig. 9(d)

Elements	C	O	Cr	Co	W	Total
Weight percentage	22.77 ± 2.55	31.71 ± 3.80	14.97 ± 0.45	16.92 ± 0.48	13.63 ± 0.40	100
Atomic percentage	41.88± 4.69	43.78± 5.25	6.36± 0.19	6.34± 0.18	1.64± 0.05	100

4. Conclusions

In this work, the corrosion performance of WC-10Co4Cr coating was studied in the simulated seawater drilling fluid under high pressure. Therefore, the corrosion test was conducted to compare the 35CrMo steel substrate, the conventional coating and the bimodal coating. From the results obtained from this work, the following conclusions can be drawn:

(1) Compared with conventional coatings, bimodal coatings have denser structure, higher microhardness and lower porosity.

(2) In the simulated seawater drilling fluid, WC-10Co4Cr coating has a better corrosion resistance than substrate, which can enhance protection for the substrate effectively. The bimodal coatings have better corrosion resistance due to more uniform microstructure than the conventional coatings.

(3) The micro-galvanic corrosion caused by the micro-galvanic cells between the WC phase and the CoCr binder phase is the primary corrosion mechanism of the coating in the simulated seawater drilling fluid. Besides, the electrolyte under the high pressure is more penetrable, so the crevice corrosion also exists.

(4) The corrosion morphologies of the coating are pitting and spalling, and due to the short immersion time, only the surface and subsurface of the coatings are corroded, the electrolyte does not proceed into the bulk of the coatings.

Acknowledgements

This project is supported by the National Key Technology R&D Program of China (Grant No. 2018YFC0603403), National Natural Science Foundation of China (Grant No. 41772389, 41872183), the Pre-Research Program in National 13th Five-Year Plan (Grant No. 61409230603), and Joint Fund of Ministry of Education for Pre-research of Equipment for Young Personnel Project (Grant No. 6141A02033120).

References

[1] J.R. Hein, K. Mizell, A. Koschinsky, T.A. Conrad, Deep-ocean mineral deposits as a source of critical metals for high- and green-technology applications: Comparison with land-based resources, Ore. Geol. Rev. 51 (2013) 1-14.

[2] X.Y. Cui, C.B. Wang, J.J. Kang, W. Yue, Z.Q. Fu, L.N. Zhu, Influence of the corrosion of saturated saltwater drilling fluid on the tribological behavior of HVOF WC-10Co4Cr coatings, Eng. Fail. Anal. 71 (2017) 195-203.

[3] M. Liu, S.J. Luo, Y. Shen, X.Z. Lin, Corrosion fatigue crack propagation behavior of S135 high-strength drill pipe steel in H_2S environment, Eng. Fail. Anal. 97 (2019) 493-505.

[4] M.R. Thakare, J.A. Wharton, R.J.K. Wood, C. Menger, Exposure effects of alkaline drilling fluid on the microscale abrasion–corrosion of WC-based hardmetals, Wear 263 (2007) 125-136.

[5] W.B. Qin, J.S. Li, Y.Y. Liu, J.J. Kang, L.N. Zhu, D.F. Shu, P. Peng, D.S. She, D.Z. Meng, Y.S. Li, Effects of grain size on tensile property and fracture morphology of 316L stainless steel, Mater. Lett. 254 (2019) 116–119.

[6] G. Bolelli, B. Bonferroni, G. Coletta, L. Lusvarghi, F. Pitacco, Wear and corrosion behaviour of HVOF WC–CoCr/CVD DLC hybrid coating systems deposited onto aluminium substrate, Surf. Coat. Technol. 205 (2011) 4211-4220.

[7] M. Szala, T. Hejwowski, Cavitation Erosion Resistance and Wear Mechanism Model of Flame-Sprayed Al2O3-40%TiO2/NiMoAl Cermet Coatings, Coatings 8 (2018) 254.

[8] S. Hong, Y.P. Wu, W.W. GAO, J.F. Zhang, Y.G. Zheng, Y. Zheng, Slurry erosion-corrosion resistance and microbial corrosion electrochemical characteristics of HVOF sprayed WC-10Co-4Cr coating for offshore hydraulic machinery, Int. J. Refract. Met.

Hard Mat. 74 (2018) 7–13.

[9] N. Liu, L.Q. Wang, S.H. Wu, D.S. Likhachev, Research on cavitation erosion and wear resistance performance of coatings, Eng. Fail. Anal. 55 (2015) 208–223.

[10] X.B. Liu, J.J. Kang, W. YUE, Z.Q. Fu, L.N. Zhu, D.S. She, J Liang, C.B. Wang, Performance evaluation of HVOF sprayed WC-10Co4Cr coatings under slurry erosion, Surf. Eng, 35 (2019) 816-825.

[11] J.M. Perry, A. Neville, T. Hodgkiess, A Comparison of the Corrosion Behavior of WC-Co-Cr and WC-Co HVOF Thermally Sprayed Coatings by In Situ Atomic Force Microscopy (AFM), J. Therm. Spray Technol. 11 (2002) 536.

[12] G. Bolelli, R. Giovanardi, L. Lusvarghi, T. Manfredini, Corrosion resistance of HVOF-sprayed coatings for hard chrome replacement, Corros. Sci. 48 (2006) 3375–3397.

[13] S. Hong, Y.P. Wu, Y.G. Zheng, B. Wang, W.W. Gao, J.R. Lin, Microstructure and electrochemical properties of nanostructured WC–10Co–4Cr coating prepared by HVOF spraying, Surf. Coat. Technol. 235 (2013) 582-588.

[14] Q. Wang, S.Y. Zhang, Y.L. Cheng, J. Xiang, X.Q. Zhao, G.B. Yang, Wear and corrosion performance of WC–10Co4Cr coatings deposited by different HVOF and HVAF spraying processes, Surf. Coat. Technol. 218 (2013) 127–136.

[15] M.M. Stack, M.T. Mathew, C. Hodge, Micro–abrasion–corrosion interactions of Ni–Cr/WC based coatings: approaches to construction of tribo–corrosion maps for the abrasion–corrosion synergism, Electrochim. Acta 56 (2011) 8249–8259.

[16] C.X. Ouyang, S.G. Zhu, D.Y. Li, Corrosion and corrosive wear behavior of WC–MgO composites with and without grain–growth inhibitors, J. Alloy. Compd. 615 (2014) 145–155.

[17] J.A. Picas, E. Rupérez, M. Punset, A. Forn, Influence of HVOF spraying

parameters on the corrosion resistance of WC–CoCr coatings in strong acidic environment, Surf. Coat. Technol. 225 (2013) 47–57.

[18] G.C. Saha, T.I. Khan, The Corrosion and Wear Performance of Microcrystalline WC-10Co-4Cr and Near-Nanocrystalline WC-17Co High Velocity Oxy-Fuel Sprayed Coatings on Steel Substrate, Metall. Mater. Trans. A. 41 (2010) 3000.

[19] G.C. Saha, T.I. Khan, G.A. Zhang, Erosion–corrosion resistance of microcrystalline and near-nanocrystalline WC–17Co high velocity oxy-fuel thermal spray coatings, Corros. Sci. 53 (2011) 2106-2114.

[20] A. Lekatou, D. Sioulas, A.E. Karantzalis, D. Grimanelis, A comparative study on the microstructure and surface property evaluation of coatings produced from nanostructured and conventional WC–Co powders HVOF-sprayed on Al7075, Surf. Coat. Technol. 276 (2015) 539.

[21] A.K. Basak, J.P. Celis, M. Vardavoulias, P. Matteazzi, Effect of nanostructuring and Al alloying on corrosion behaviour of thermal sprayed WC-Co coatings, Surf. Coat. Technol. 206 (2012) 3508–3516.

[22] J.M. Guilemany, S. Dosta, J.R. Miguel, The enhancement of the properties of WC-Co HVOF coatings through the use of nanostructured and microstructured feedstock powders, Surf. Coat. Technol. 201 (2006) 1180.

[23] J.M. Guilemany, J. Nin, S. Dosta, J.R. Miguel, Study of the Properties of WC-Co Nanostructured Coatings Sprayed by High-Velocity Oxyfuel, J. Therm. Spray Technol. 14 (2005) 405

[24] A.K. Basak, J.P. Celis, M. Vardavoulias, P. Matteazzi, Effect of nanostructuring and Al alloying on friction and wear behaviour of thermal sprayed WC–Co coatings, Surf. Coat. Technol. 206 (2012) 3508.

[25] H.J.C. Voorwald, R.C. Souza, W.L. Pigatin, M.O.H. Cioffi, Evaluation of WC–

17Co and WC–10Co–4Cr thermal spray coatings by HVOF on the fatigue and corrosion strength of AISI 4340 steel, Surf. Coat. Technol. 190 (2005) 155–164.

[26] S.H. Li, Z.X. Guo, J. Xiong, Y. Lei, Y.X. Li, J. Tang, J.B. Liu, J.L. Ye, Corrosion behavior of HVOF sprayed hard face coatings in alkaline-sulfide solution, Appl. Surf. Sci. 416 (2017) 69-77.

[27] V.P.S. Sidhu, K. Goyal, R. Goyal. An investigation of corrosion resistance of HVOF coated ASME SA213 T91 boiler steel in an actual boiler environment, Anti-Corros. Methods Mater. 64 (2017) 499-507.

[28] B.H. Kear, G. Skandan, R.K. Sadangi. Factors controlling decarburization in HVOF sprayed nano-WC/Co hardcoatings, Scr. Mater. 44 (2001) 1703-1707.

[29] A. Lekatou, A.K. Sfikas, A.E. Karantzalis, D. Sioulas, Microstructure and corrosion performance of Al-32%Co alloys, Corros. Sci. 63 (2012) 193.

[30] S. Hong, Y.P. Wu, Y.G. Zheng, B. Wang, W.W. Gao, G.Y. Li, G.B. Ying, J.R. Lin, Effect of Spray Parameters on the Corrosion Behavior of HVOF Sprayed WC-Co-Cr Coatings, J. Mater. Eng. Perform. 23 (2014) 1434-1439.

[31] T. Sudaprasert, P.H. Shipway, D.G. Mccartney, Sliding wear behaviour of HVOF sprayed WC–Co coatings deposited with both gas-fuelled and liquid, Wear 255 (2003) 943-949.

[32] D.A. Stewart, P.H. Shipway, D.G. McCartney, Microstructural evolution in thermally sprayed WC–Co coatings: comparison between nanocomposite and conventional starting powders, Acta Mater. 48 (2000) 1593–604.

[33] R.J.K. Wood, R. Manish, Tribology of thermal sprayed WC–Co coatings, Int. J. Refract. Met. Hard Mat. 28 (2010) 82-94.

[34] M.R. Thakare, J.A. Wharton, R.J.K. Wood, C. Menger, Exposure effects of strong alkaline conditions on the microscale abrasion–corrosion of D-gun sprayed WC–10Co–

4Cr coating, Tribol. Int. 41 (2008) 629-639.

[35] B. Yin, H.D. Zhou, D.L. Yi, J.M. Chen, F.Y. Yan, Microsliding wear behaviour of HVOF sprayed conventional and nanostructured WC–12Co coatings at elevated temperatures, Surf. Eng. 26 (2010) 469.

[36] G. Bolelli, V. Cannillo, L. Lusvarghi, S. Ricco, Mechanical and tribological properties of electrolytic hard chrome and HVOF-sprayed coatings, Surf. Coat. Technol. 200 (2006) 2995.

[37] J.E. Cho, S.Y. Hwang, K.Y. Kim, Corrosion behavior of thermal sprayed WC cermet coatings having various metallic binders in strong acidic environment, Surf. Coat. Technol. 200 (2006) 2653-2662.

[38] M. Barletta, G. Bolelli, B. Bonferroni, L. Lusvarghi, Wear and Corrosion Behavior of HVOF-Sprayed WC-CoCr Coatings on Al Alloys, J. Therm. Spray Technol. 5 (2006) 106-117.

[39] C. Liu, R.I. Revilla, Z. Liu, D. Zhang, X. Li, H. Terryn, Effect of inclusions modified by rare earth elements (Ce, La) on localized marine corrosion in Q460NH weathering steel, Corrosion Sci. 129 (2017) 82-90.

[40] Z.Y. Liu, X.G. Li, Y.F. Cheng, Understand the occurrence of pitting corrosion of pipeline carbon steel under cathodic polarization, Electrochim. Acta 60 (2012) 259-263.

[41] G.C. Saha, T.I. Khan, The Corrosion and Wear Performance of Microcrystalline WC-10Co-4Cr and Near-Nanocrystalline WC-17Co High Velocity Oxy-Fuel Sprayed Coatings on Steel Substrate, Metall. Mater. Trans. A-Phys. Metall. Mater. Sci. 41 (2010) 3000-3009.

[42] Y. Wang, S.L. Jiang, Y.G. Zheng, W. Ke, W.H. Sun, J.Q. Wang, Effect of porosity sealing treatments on the corrosion resistance of high-velocity oxy-fuel (HVOF)-sprayed Fe-based amorphous metallic coatings, Surf. Coat. Technol. 206 (2011) 1307-

1318.

[43] W.K. Hao, Z.Y. Liu, W. Wu, X.G. Li, C.W. Du, D.W. Zhang, Electrochemical characterization and stress corrosion cracking of E690 high strength steel in wet-dry cyclic marine environments, Mater. Sci. Eng. A-Struct. Mater. Prop. Microstruct. Process. 710 (2018) 318-328.

[44] Q. Hou, Z.Y. Liu, C.T. Li, X.G. Li, The mechanism of stress corrosion cracking of Alloy 690TT in a caustic solution containing lead, Corrosion Sci. 128 (2017) 154-163.

[45] Q. Wang, S.Y. Zhang, Y.L. Cheng, J. Xiang, X.Q. Zhao, G.B. Yang, Wear and corrosion performance of WC-10Co4Cr coatings deposited by different HVOF and HVAF spraying processes, Surf. Coat. Technol. 218 (2013) 127-136.

[46] A. Dwars, W. Kochanowski, B. Schramm, F. Sehr, Application of thermally sprayed coatings of the type WC/CoCr in reverse osmosis processes for seawater desalination, Mater. Corros. 59 (2008) 870-877

[47] A. Lekatou, D. Zois, A.E. Karantzalis, D. Grimanelis, Electrochemical behaviour of cermet coatings with a bond coat on Al7075: Pseudopassivity, localized corrosion and galvanic effect considerations in a saline environment, Corros. Sci. 52 (2010) 2616.

[48] A. Neville, T. Hodgkiess, The corrosion behaviour and microstructure of two thermal spray coatings, Surf. Eng. 12 (1996) 303–312.

[49] M. Magnani, P.H. Suegama, A.A.C. Recco, J.M. Guilemany, C.S. Fugivara, A.V. Benedetti, WC-CoCr Coatings Sprayed by High Velocity Oxygen-Fuel (HVOF) Flame on AA7050 Aluminum Alloy: Electrochemical Behavior in 3.5% NaCl Solution, Mater. Res. 10 (2007) 377-385.

[50] M. Takeda, N. Morihiro, R. Ebara, Y. Harada, R. Wang, M. Kido, Corrosion behavior of thermally sprayed WC coating in Na_2SO_4 aqueous solution. Mater. Trans. 43 (2002) 2860–2865.

Highlights:

- WC-10Co4Cr coatings with bimodal structures have superior properties than conventional structures.
- WC-10Co4Cr coatings have a better corrosion resistance than substrate.
- The bimodal coatings have better corrosion resistance than conventional coatings.
- The micro-galvanic corrosion is the primary corrosion mechanism of the coatings, and the crevice corrosion also exists.